Urban morphology modulates thunderstorm process and associatied cloud-to-ground lightning activity over Beijing metropolitan region

Tao Shi[1,2], Yuanjian Yang[2*], Gaopeng Lu[1], Zuofang Zheng[3], Yucheng Zi[1], Ye Tian[4], Lei Liu[2], Simone Lolli[5]

[1]School of Earth and Space Sciences, University of Science and Technology of China, Hefei, 241000, China
[2]Collaborative Innovation Center on Forecast and Evaluation of Meteorological Disasters, Nanjing University of Information Science and Technology, Nanjing, 210000, China
[3]Institute of Urban Meteorology, China Meteorological Administration, Beijing, 100000, China
10 [4]Beijing Meteorological Observation Center, Beijing, 100000, China.
[5]CNR-IMAA, Contrada S. Loja, 85050 Tito Scalo (PZ), Italy

Correspondence to: Prof. Yuanjian Yang (yyj1985@nuist.edu.cn)

Abstract. The effect of urban barriers may have a significant impact on the patterns of thunderstorm processes and lightning activity, but there is still a lack of comprehensive mechanical explanations. The observational analysis carried out in this 15 study found that cloud-to-ground (CG) lighting activity tends to cluster around the outer boundaries of the mega cities, while, on the opposite, CG gathers within the small-sized city. When a squall line originating from a type of mesoscale convective system (MCS) known as '0713' passed through the built-up area, the barrier effect of the rough underlying surface contributed to the separation of the cold pool. This led to weakening of vertical airflow and breaking of the convergence line, ultimately triggering the bifurcation of the thunderstorm. Simulation results complement these observations. When buildings 20 outside the 5 Ring Road (RR) are replaced with bare soil, the separation of the cold pool is minimized. Furthermore, the density of the buildings also influenced the strength of the barrier effect. Therefore, the specific urban morphologies were identified as a critical factor in modulating cloud-to-ground (CG) lighting activity and the organization process of thunderstorms. This study offers a fundamental foundation and technical support for predicting and assessing urban cloud-to-ground (CG) lightning risks. It holds significant implications for understanding excess urban warming, its prediction and 25 assessment, and the resulting thermal risk, influenced by factors such as ventilation, sea breezes, and the geophysical environment in coastal cities.

1 Introduction

As urbanization progressed, lightning events emerged as a significant hazard to city safety and social development, presenting a serious weather-related risk (Westcott and Nancy, 1995; Pinto et al., 2004). Among these events, cloud-to-30 ground (CG) lightning poses the greatest risk to both ground-based objects and population. The scientific consensus on the enhancement of the urban thermal effect on lightning and thunderstorms has been widely recognized (Shepherd., 2005;

Wang et al., 2018; Yue et al., 2019; Wang et al., 2021; Shi et al., 2022). The thermal effect increases the boundary layer height above cities and the vertical mixing height (Xu et al., 2013; Sun et al., 2021). The vertical mesoscale cutting resulting from temperature differences between urban and suburban areas serves as a key prerequisite for the development of the
35   convective system. (Farias et al., 2014; Sun et al., 2013).

Furthermore, different studies s have also recognized the impact of urban underlying morphologies on lightning activity and thunderstorm processes (Bornstein and LeRoy, 1990; Dai et al., 2005; Shi et al., 2022). Buildings act as frictional barriers that alter the horizontal wind field, enhancing convergence and upward movement in the upstream direction (Jin and Shepherd, 2005), thereby enhancing thunderstorm system development to some extent (Yin et al., 2020). In general, the
40   intensity of airflow "climbing" movement is relatively weak (Zu et al., 2016). Previous studies have suggested that, when thunderstorms pass over cities, the barrier effect can lead to bifurcation and diversion of the thunderstorm system. (Bornstein and LeRoy, 1990; Lorenz et al., 2019). Additionally, peak areas of lightning and rainfall tend to concentrate in the outskirts of the metropolitan areas (Stallins and Bentley, 2006; Dou et al., 2015; Shi et al., 2022). A recent study analyzing thunderstorms passing over Nanjing found that the urban barrier effect primarily dominates the spatial pattern of lightning
45   density (Yang et al., 2021). However, other researchers point out that, despite that the buildings in the Beijing metropolitan area splitting the squall line into convective cells, the barrier effect on intense convection is less significant compared to the thermal effect (Miao et al., 2011). In summary, there is still a lack of comprehensive explanation regarding the mechanisms behind how the urban morphologies alter CG lightning activity and thunderstorm processes.

With a population exceeding 20 millions, a built-up area spanning approximately 1500 km^2, and a gross domestic product
50   (GDP) exceeding 4 trillion, Beijing metropolitan area stands as the most urbanized city within the urban agglomeration of Beijing-Tianjin-Hebei (National Bureau of Statistics of the People's Republic of China, 2021). In recent years, Beijing metropolitan area has been repeatedly impacted by severe convective weather events, leading to significant economic and social disruptions (Qie et al., 2021). The study focused on the Beijing metropolitan area as a research area and aimed to analyze the impact of the urban soil on the CG lighting activity and the thermal-dynamic structure of thunderstorms. Using
55   observation data and numerical modeling techniques, our present work will provide valuable theoretical insight and technical support to improve the prediction, nowcasting, warning, and risk assessment of urban CG lightning.

2 IntroductionData and methodology

2.1 Study Area

The Beijing-Tianjin-Hebei urban agglomeration, located on the north China plain, is one of three major urban
60   agglomerations in China. At its core lies the Beijing mtropolitan area, which serves as the political, economic, cultural and scientific center of China. With a dense population and rapid urbanization, the built up areas of Beijing have expanded to more than 1500 km^2, covering most of the southeastern plain regions. Thunderstorms in Beijing typically originate from the western mountains and spread to the northeast and southeast plains (Chen et al., 2012). When interacting with warm and

humid airflows southward, these thunderstorms often intensify forming squall lines (Sun and Yang, 2008; Xiao et al., 2017).

65 Zhangjiakou (ZJK) and Tianjin (TJ) are located in the northwest and southeast of Beijing, respectively. Both regions show a similar climate to Beijing, characterized by a temperate continental monsoon climate with frequent, short-lived, and hot thunderstorms during summer. ZJK is located approximately 180 kilometers from BJ, with a built-up area sof 104.2 km^2, only one-tenth of BJ built-up area. It is considered to be one of the least urbanized cities within the Beijing-Tianjin-Hebei urban agglomeration. In comparison, TJ built-up area , situated just 60 kilometers from BJ, spans approximately 605.42 km^2.

70 Therefore, Beijing (BJ), Zhangjiakou (ZJK) and Tianjin (TJ) show different scales of urbanization and for this reason are then used to explore the effects of urban morphology on lightning and storm processes.
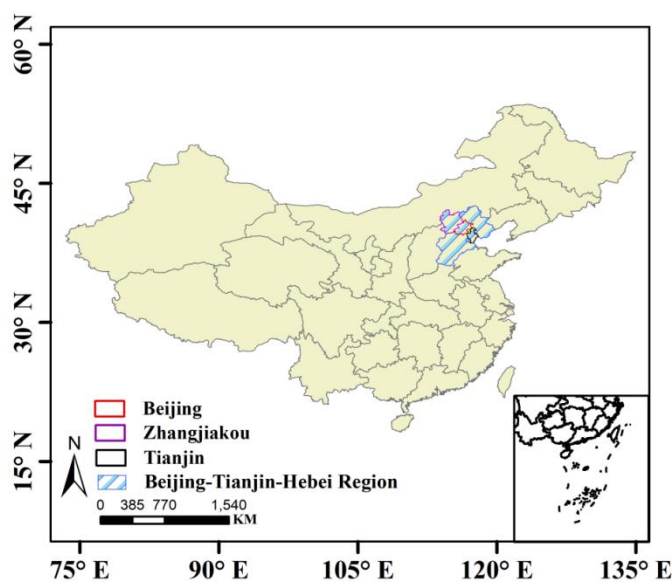
Figure 1: Overview of the study area.

75 **2.2 Data**

The State Grid Lightning Network (SGLNET) is utilized to collect lightning location datasets, which include longitude and latitude, GPS time, peak current, polarity, and other relevant information (Wang et al., 2021). In this study, we utilized the SGLNET lightning location data. Lightning events are detected using magnetic direction-finding and time-of-arrival (MDF-TOA) technologies within the SGLNET, achieving a detection efficiency of 94% and a location error of 489 m, respectively

80 (Chen et al., 2012). A previous study by Orville et al. (2002) pointed out that intra-cloud (IC) discharges may contaminate the CG lightning detection network. To address this issue, we used a screening criterion based on a peak current threshold of less than 10 kA to eliminate the potential interference from IC discharges (Schulz et al., 2005).

The hourly observation data from the auto weather station (AWS) utilized in this study were obtained from the China Meteorological Data Service Center (http://data.cma.cn/en). This datasets included near-surface air temperature, wind speed,

85 and wind direction. To address missing values in the observation sequence, we used a method previously described by Yang et al. (2011) and Xu et al. (2013). Specifically, we replaced missing values with the average of synchronous observation data from the nearest five stations, and stations with excessive erroneous records were excluded. For this study, we selected 54 AWSs, which are evenly distributed throughout the research area, to analyze the temporal-spatial pattern of the near-surface thermal-dynamic field in the Beijing metropolis.

90 To investigate the process of evolution of thunderstorms, we utilized the composite reflectivity (CR) product from the S-band Doppler radar at the Beijing Nanjiao Observatory. These radar data were relevant for analyzing the 13 July 2017 thunderstorm event ("0713"). In addition, to gain a broader understanding of the synoptic background of thunderstorms, we utilized sounding data from the Beijing Nanjiao Observatory. These sounding data were collected at 02:00, 08:00, 14:00, and 20:00 Beijing time every day.

95 Stewart and Oke (2012) introduced the concept of local climate zones (LCZs), which refers to areas with identical land use, similar spatial morphology, building materials, and human activities, on a scale ranging from a few hundred to a few thousand meters. The LCZ datasets used in this paper were provided by the Institute of Urban Meteorology, China Meteorological Administration. The fundamental types and quantitative descriptive indicators of these LCZ datasets are outlined in Table 1.

100

Table 1: Different categories of LCZ datasets.

Schematic diagram of urban morphology	Characterization of Urban Morphology	Indicators of LCZ categories
LCZ 1: Compact high-rise	The building are taller than 10 stories. High density of buildings and ground cover mostly hard pavement with little vegetation.	Aspect ratio >2 Sky view factor: 0.2-0.4 Building surface fraction: 40-60 Impervious surface fraction: 40-60 Pervious surface fraction < 10 Height of roughness elements >25
LCZ 2: Compact mid-rise	Building heights span from 3 to 9 stories. High density of buildings of buildings and ground cover mostly hard pavement with little vegetation.	Aspect ratio: 0.75-2 Sky View Factor: 0.3-0.6 Building surface fraction: 40-70 Impervious surface fraction: 30-50 Pervious surface fraction <20 Height of roughness elements: 10-25
LCZ 3: Compact low-rise	Building heights ranging from 1 to 3 stories. High density of buildings and	Aspect ratio: 0.75-1.5 Sky view factor: 0.2-0.6
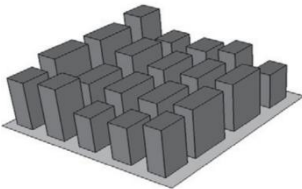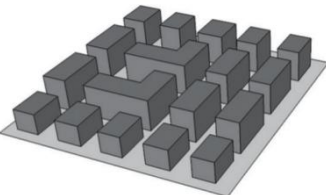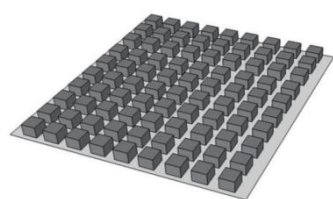
ground cover mostly hard pavement with little vegetation.

Building surface fraction: 40-70

Impervious surface fraction: 20-50

Pervious surface fraction <30

Height of roughness elements: 3-10

LCZ 4: Open High-rise
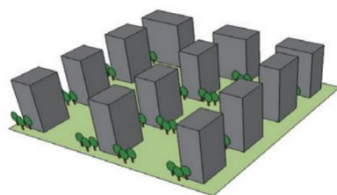
Building heights of 10 stories or more. Low density of buildings and low ground cover mostly permeable ground or vegetation.

Aspect ratio: 0.75-1.25

Sky View Factor: 0.5-0.7

Building surface fraction: 20-40

Impervious surface fraction: 30-40

Pervious surface fraction: 30-40

Height of roughness elements >25

LCZ 5: Open mid-rise
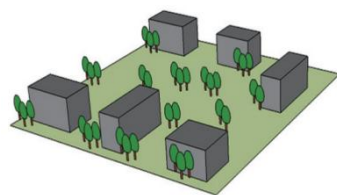
Building heights in the range of 3-10. Low density of buildings and low ground cover mostly permeable ground or vegetation.

Aspect ratio: 0.3-0.75

Sky view factor: 0.5-0.8

Building surface fraction: 20-40

Impervious surface fraction: 30-50

Pervious surface fraction: 20-40

Height of roughness elements: 10-25

LCZ 6: Open low-rise
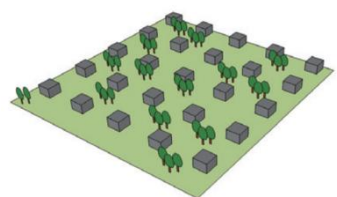
Building heights ranging from 1 to 3 stories. The low density of buildings and the ground cover is mostly permeable ground or vegetation.

Aspect ratio: 0.3-0.75

Sky View Factor: 0.6-0.9

Building surface fraction: 20-40

Impervious surface fraction: 20-50

Pervious surface fraction: 30-60

Height of roughness elements: 3-10

2.3 Numerical simulation scheme

The numerical model in this paper adopted Weather Research and Forecasting (WRF) version 4.0, coupled with the single layer Urban canopy scheme (SLUCM), and designed a 5-km, 1-km, and 200-m triple nested grid in the horizontal direction (Figure. 2).

The numerical model utilized in this paper was Weather Research and Forecasting (WRF) version 4.0, which was coupled with the Single Layer Urban Canopy Scheme (SLUCM). It featured a horizontal grid configuration with 5-km, 1-km, and 200-m nested grids (Figure. 2).
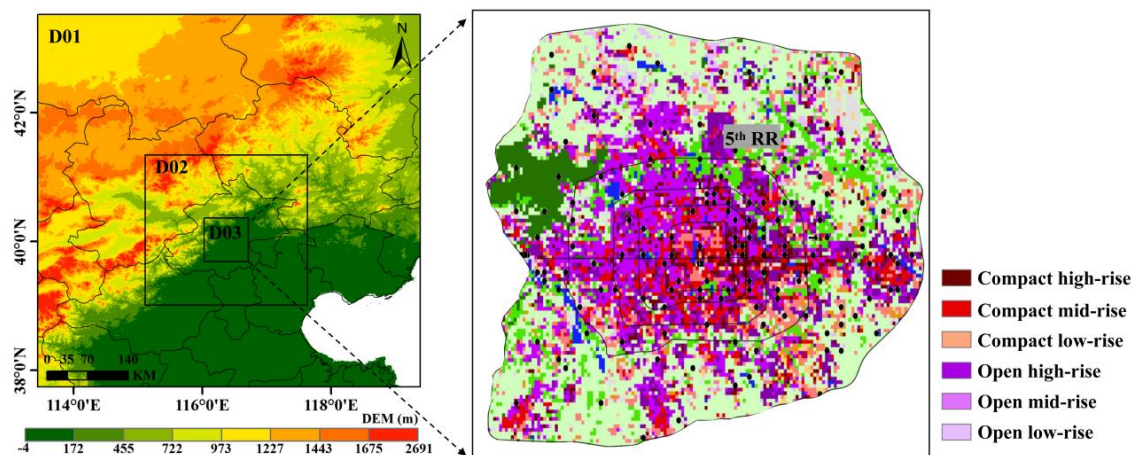
Figure 2: Terrain height distribution and the building types of the WRF mesoscale numerical model.

The underlying surface data encompassed land use and urban canopy datasets with a resolution of 10 meters. This model employed the WRF Single Moment 6-class microphysical process scheme (WSM6), the rapid radiative transfer longwave radiation scheme (RRTM), the Dudhia shortwave radiation scheme, the step-mountain similarity theory near-surface layer scheme, and the BouLac boundary layer scheme (Lim and Hong, 2010; Lacono et al., 2008; Janjic, 1994; Melin, 2017; Tewari et al., 2004). The parameterization schemes utilized in the simulations are shown in the Table 2.

Table 2: Parameterization schemes of the WRF model in this paper.

Numerical and Physical Process	Schemes
Microphysics	WSM6
Longwave radiation	RRTM
Shortwave radiation	Dudhia
Planetary boundary layer	BouLac
Surface layer	Step-mountain
Urban canopy layer	UCM

The simulation began at 00:00 on July 13th, 2017, and lasted for 24 hours. The length and area of the 5th Ring Road (RR) in Beijing are approximately 98.6 km and 600 km2, respectively. To more accurately assess the impact of urban morphologies on the dynamic and thermal effects, we conducted five sets of experiments. These included a control experiment (EXP1) and four sensitivity tests (EXP2, EXP3, EXP4, EXP5). The specifics of these experiments were described in the Table 3.

Table 3: Description of different experiments.

Experiment	Style	Description
EXP1	Controlled experiment	Actual Land Use Situation and Building Structure
EXP2	Sensitive experiment	Outside the 5th RR with only bare soil
EXP3	Sensitive experiment	The built-up area with only bare land
EXP4	Sensitive experiment	The built-up area with only open-rise
EXP5	Sensitive experiment	The built-up area with only compact-rise

3 Results

130 ## 3.1 CG lightning activity around the built-up area

Spatial analysis of long-term lightning location data offers valuable insights into the climatic patterns of lightning activity, which constitutes a crucial component of urban lightning disaster research. In this section, a thorough examination of the spatial characteristics of CG lightning activity was conducted within the built-up areas of Beijing using SGLNET data.
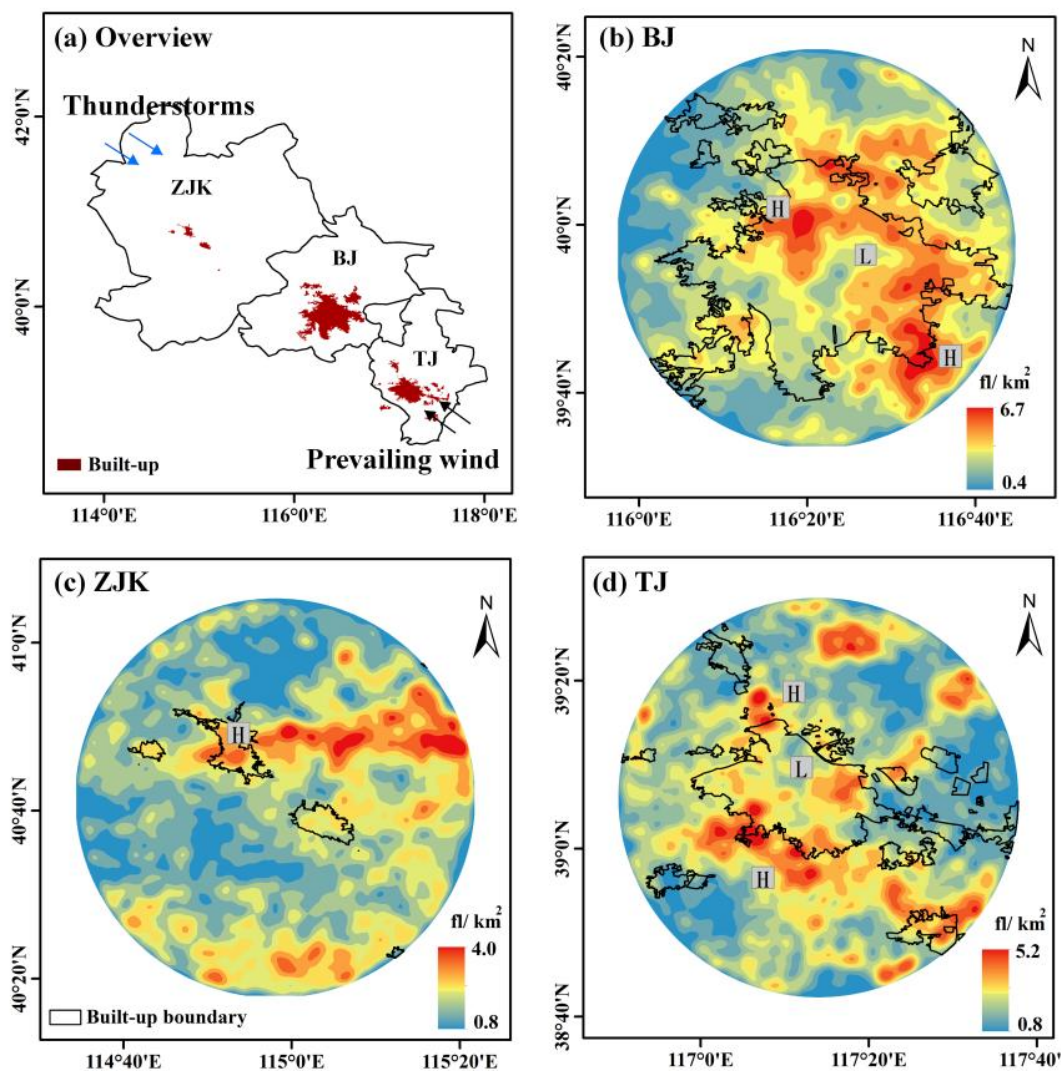
Figure: 3 Overview of the areas built up (a). The spatial pattern of flash density in the built-up areas of Beijing (BJ) (b), Zhangjiakou (ZJK) (c), Tianjin(TJ) (d) from 2010 to 2017.

In Figure 3b, SGLNET recorded more than 50,000 CG flashes in the built-up area of Beijing (BJ) during the study period. It is clear that the distribution of CG lights in the built area is uneven.There were clusters of abundant flashes are visible and concentrated upwind and downwind of the built-up area (marked as H), with an average and maximum densities reaching 4 fl/km^2 and 6 fl/km^2, respectively. It should be noted that the CG flash in the city center was sparse (marked as L), with an average density of less than 1 fl/km^2. This pattern was similar to the spatial distribution of CG lightning observed in the United States, more precisely in Houston (Steiger and Orville, 2002) and Atlanta (Stallins and Bentley, 2006; Stallins and Rose, 2008). Therefore, we can speculate that exists   a potential barrier effect that alters the pattern of CG lightning within

145   the built-up area of Beijing. As shown in Figure 3c, the entire built-up area of Zhangjiakou (ZJK) was mainly covered by high CG lightning density (H) region, with a peak density of 3.6 fl/km^2 in the city center. Examining Figure 3d, it is evident that a significant concentration of CG lightning events occurrs along the outskirts of the built-up area of Tianjin (TJ), with a maximum CG lightning density of 5.2 fl/km^2. Similar to Beijing, the center of the built-up area in Tianjin exhibited a low lightning density (L) region. Therefore, under similar climate conditions, we can speculate that the bigger the size of the

150   urban agglomerate of the city, the lower the density of CG in the city center. This is an evidence supporting the impact of theurban barrier effect.
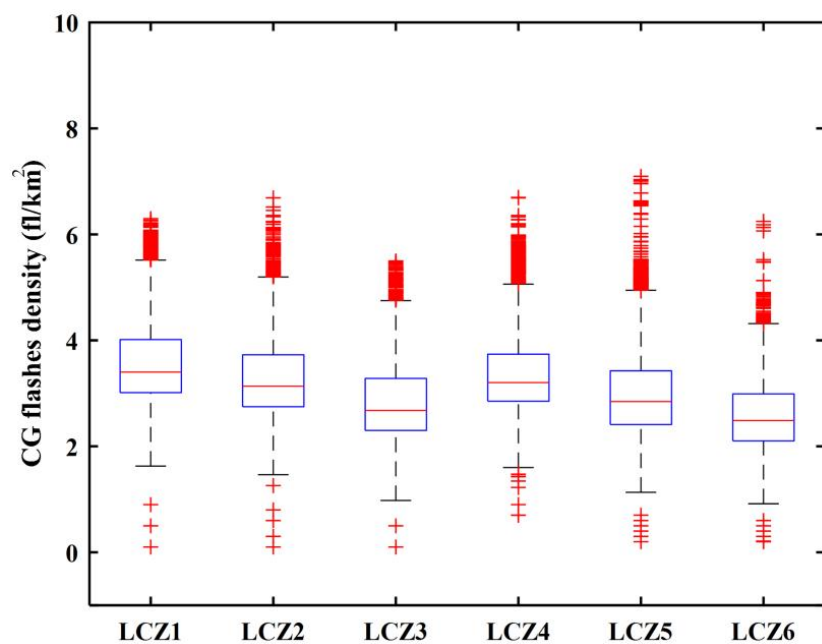
Figure 4: Statistical results of CG density for different types of LCZ.

155   Utilizing the spatial distribution of CG density and LCZ in Beijing, the CG activity associated with distinct LCZ types were detailed in statistics, aiming to gain a deeper understanding of the relationship between lightning occurrences and the characteristics of various built environments in the city. As illustrated in Figure 4, there were 3,525 pixels in LCZ1, 4,699 pixels in LCZ2, and 4,486 pixels in LCZ3, accounting for 10.5%, 14.0%, and 13.4% of the built-up area, respectively. The average CG density in these zones was 3.7 fl/km^2, 3.5 fl/km^2, and 3.0 fl/km^2, respectively. Furthermore, there were 7,262

160   pixels in LCZ4, 10,466 pixels in LCZ5, and 3,027 pixels in LCZ6, representing 21.7%, 31.3%, and 9.1% of the built-up area, respectively. The average CG in these zones was 3.6 fl/km^2, 3.3 fl/km^2, and 2.8 fl/km^2, respectively. It was evident that in both the compact-rise (LCZ1, LCZ2, LCZ3) and open-rise (LCZ4, LCZ5, LCZ6) areas, the density of CG increased as the height of the building increased. However, for the entire urban agglomerate, there was minimal variation in CG density between buildings of different heights.
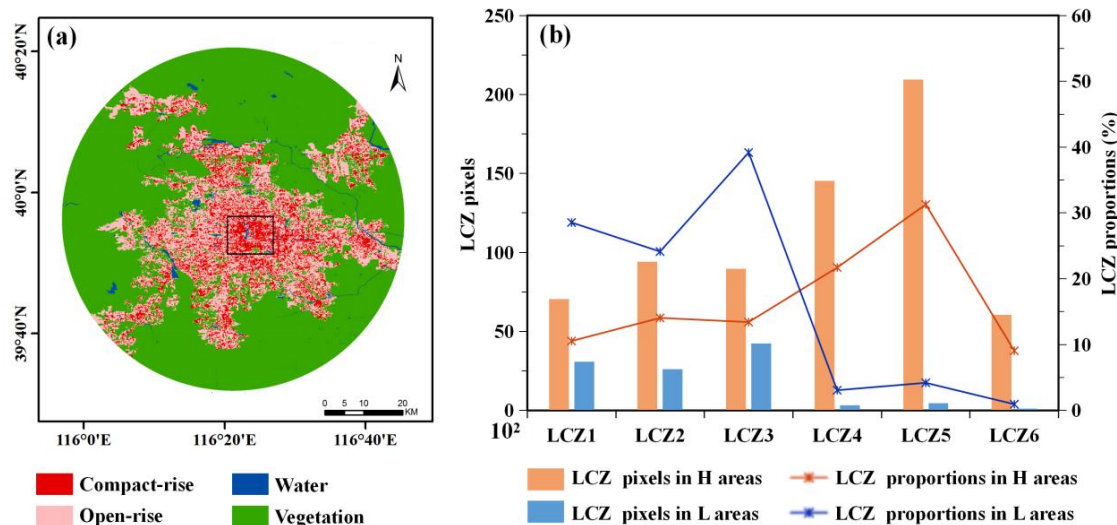
Figure 5: (a) Characteristics of the urban configuration structure dominated by density information, including compact-rise (LCZ1, LCZ2, LCZ3) and open-rise (LCZ4, LCZ5, LCZ6). (b) The configuration structure of buildings in areas with high CG density (H) and low CG density areas (L).

The impact of building density on CG lightning activity cannot be ignored. Stallins and Bentley (2006) used GIS technology to analyze the distribution characteristics of lightning in Atlanta, USA and discovered that the lightning density was low in high-density building areas. In Figure 5a, density information was used as the dominant factor to classify the urban configuration structure, which was divided into compact rise (LCZ1, LCZ2, LCZ3) and open rise (LCZ4, LCZ5, LCZ6). The edges of the built-up area in Beijing are primarily composed of.open-rise. The city center is completely constituted c compact-rise, forming large-scale compact-rise clusters with an area of approximately 100 km^2 (depicted in the black box), which was largely congruent with the low-density CG lightning areas within the built-up area. Figure 5b illustrates the distribution of various types of LCZ in the high lightning density area (H) and low lightning density area (L). The H area was primarily located in the upper and lower wind directions, spanning over 1000 km^2. Among these areas, the LCZ5 type of building area was the largest, comprising 14,524 pixels, representing 31.2% of the total area of the H area. The areas of other types of LCZ were relatively similar, accounting for 11.05%~21.2%. The L area was primarily concentrated in the urban center, spanning a total area of approximately 90 km^2. This area comprised 9,936 dense pixels, representing 91.8% of the area of the L area. The L area was mainly composed of compact-rise and contained very few open-rises in the built-up area. Consequently, the effect of the urban barrier might be associated with the scale of the built area and the density of buildings.

3.2 The evolution characteristics of the thunderstorm passing through the underlying urban surface

The CR product detected by the Beijing Nanjiao Observatory was utilized to analyze the evolution characteristics of thunderstorms passing over the built-up area. Figure 6a depicted the "0713" case, a quasi-linear convective system consisting of multiple cells that propagated from Hebei at 20:00 BJT. At this time, the thunderstorm system reached the northwest of

the built-up area. Thunderstorm cells were continuously generated, developed and merged on the right rear side of the thunderstorm system. At 21:00 BJT (Figure 6b), the thunderstorm moved to the border between the mountains and the plain and there was an evident V-shaped notch on its rear side, indicating a robust rear inflow. The area of the strong echo above

190 40 dBZ expanded further, with the echo center intensity peaking at more than 50 dBZ. It is important to note that during its propagation, the thunderstorm system broke down and gradually split into larger thunderstorm cell I and smaller thunderstorm cell II in the northwest corner of the built-up area, creating a significant barrier effect.
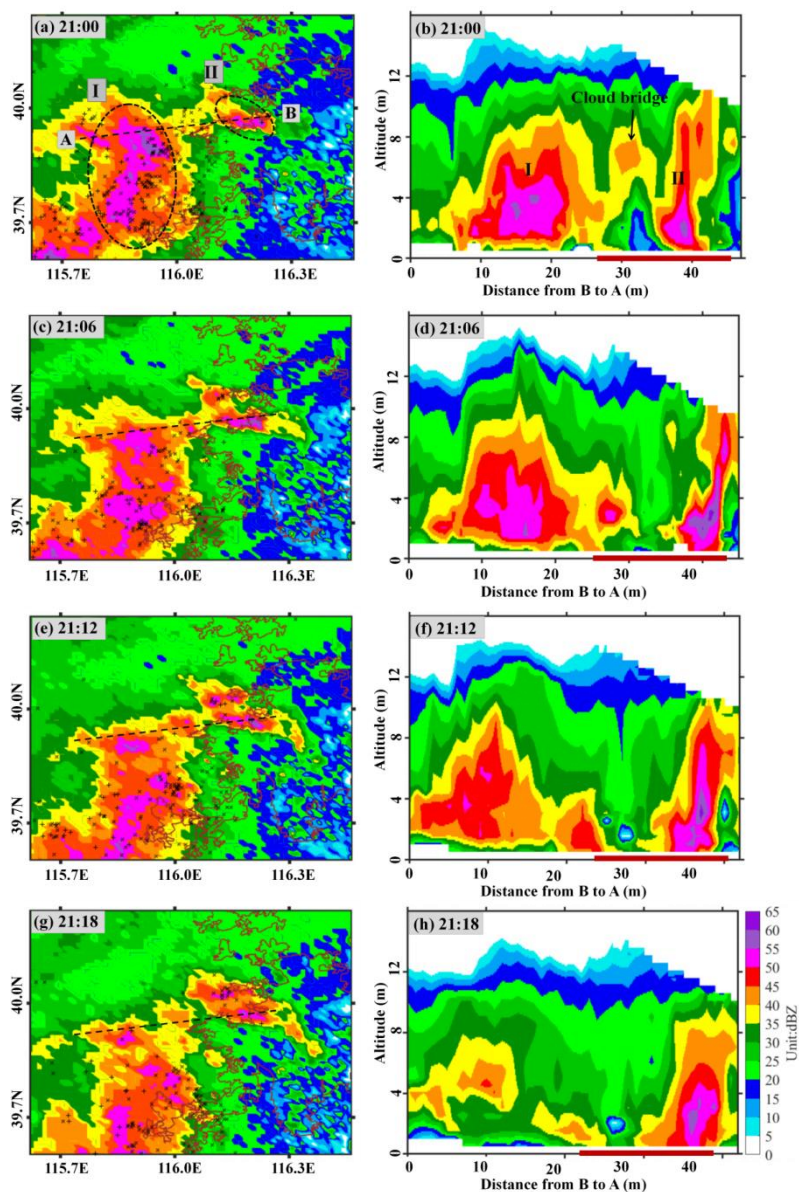
Figure 6: The echo evolution of the case "0713" during the stage of bifurcation, at 21:00 (a-b), 21:06 (c-d), 21:12 (e-f), and 21:18
195 **(g-h) BJT.**

Due to the barrier effect, the thunderstorm system began to split, with cell I and cell II remaining connected by a cloud bridge. At 21:06 (Figure 6c-6d), the echo core volume of cell I decreased, and the cloud bridge began to narrow. The echo core height of cell II expanded to 8 km, with a maximum reflectivity exceeding 65 dBZ. Furthermore, newborn cells emerged around the cloud bridge. By 21:12 (Figure 6e-6f), as the thunderstorm system approached the built-up area, the echo core of cell I and the cloud bridge weakened to 45 dBZ, while the echo core height and strong echo area of cell II continued to increase. At 21:18 (Figure 6g-6h), cell I and cell II were completely separated when the cloud bridge broke. Therefore, during "0713" case transit over the built-up area of Beijing, the urban barrier effect directly affected the spatial pattern of CG lightning activity and the organization process of the "0713" case.
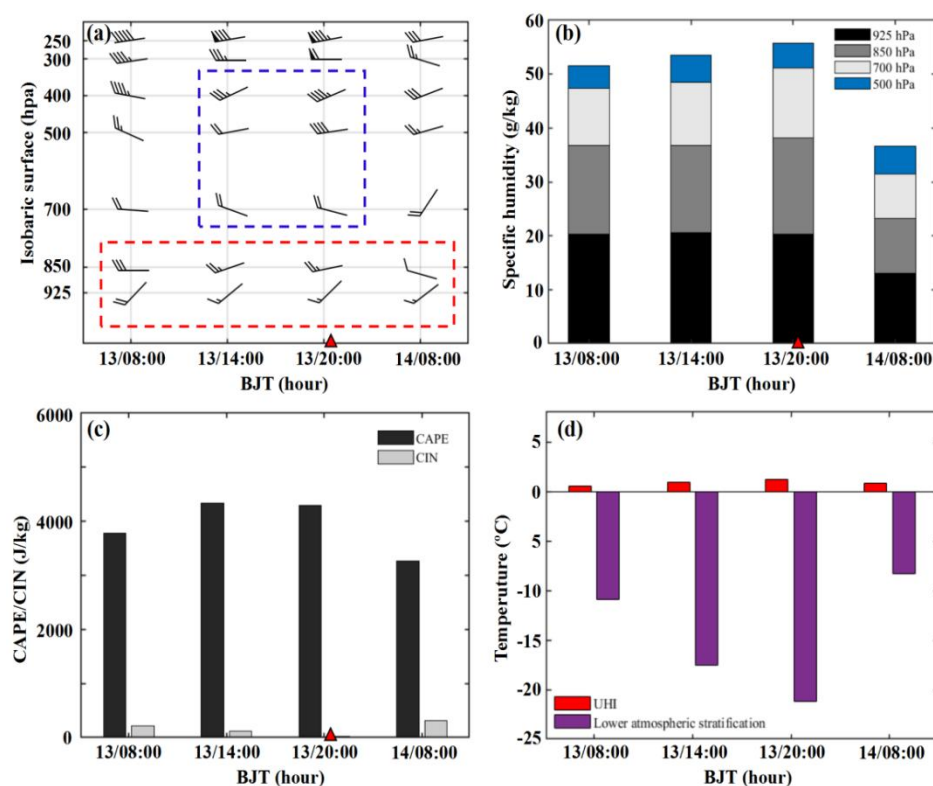
Figure 7: Wind field (a), specific humidity (b), convective effective potential energy (CAPE) and convective inhibition energy (CIN) (c), intensity of urban heat island (UHI) and lower atmospheric stratification (d). The red triangle represents the time when the "0713" case passed over the built-up area.

Through observational data, in this study we nalyzed in detai the variation characteristics of the thermal-dynamic field of the "0713" case transiting over the built-up area. At 08:00 BJT (Beijing time), the wind direction below 850 hPa in the built-up area varied clockwise with height (red box in Figure 7a), indicating a small amplitude and weak warm advection in the lower atmosphere. The intensity of urban heat island (UHI) and the pseudo-equivalent temperature between 850-925 hPa were 0.5°C and -10.9°C, respectively, indicating unstable atmospheric stratification in the lower atmosphere. The specific

humidity at 850 hPa exceeded 20 g/kg, indicating a rich water vapor content. Specific humidity at 500 hPa was

215 approximately 4 g/kg, demonstrating the characteristics of upper dry and lower wet vertical water vapor layer. The convective available potential energy (CAPE) value reached 3783.5 J/kg. At 14:00 BJT, the wind field in the middle and upper levels changed counterclockwise with height (shown in the blue box in Figure 7a), representing a strong cold advection passing over the city. As the thunderstorm system moved into the built-up area, the configuration of upper cold and lower warm increased atmospheric stratification instability. Although the UHI intensity in the built-up area was only

220 0.8ºC, the pseudo-equivalent temperature between 850 hPa and 925 hPa decreased to -17.5ºC, and the CAPE value exceeded 4000 J/kg. By 20:00 BJT, the UHI intensity, pseudo-equivalent temperature, and CAPE value continued to rise, leading to numerous CG lightning events initiated at the edge of the built-up area.
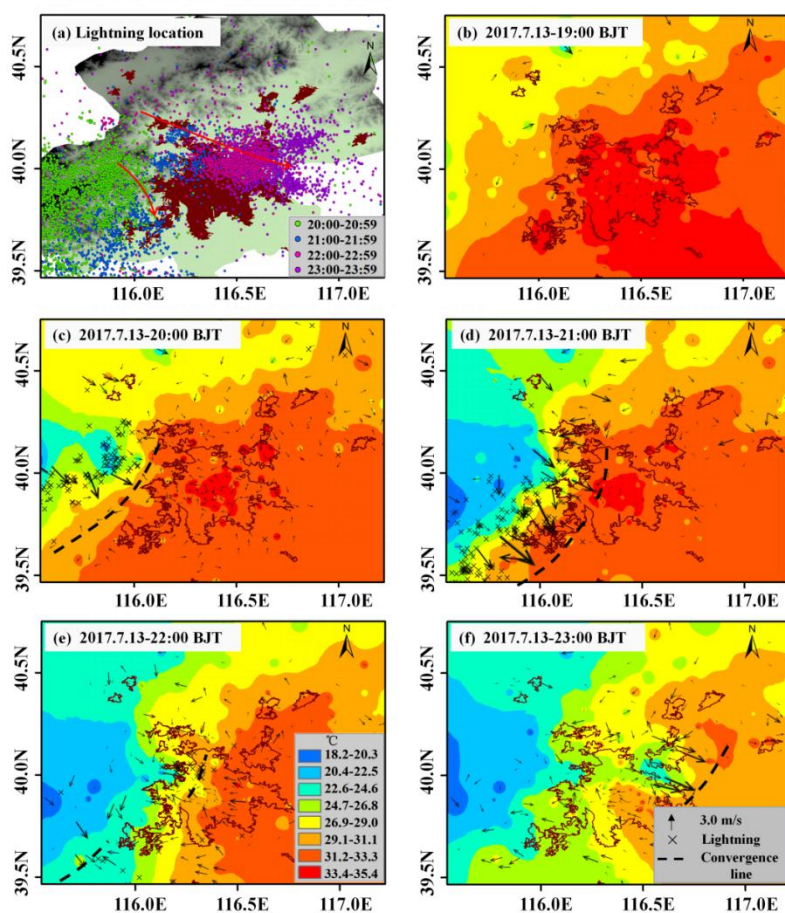
Figure 8: The spatial pattern of spatial pattern of CG lightning (a) and the the near-surface thermal-dynamic field (b-f) of the case
225 **"0713" transiting over the built-up area.**

The AWS data were further utilized to study the evolution characteristics of the near-surface thermal-dynamic field. At 19:00 BJT (Figure 8b), the entire plain area of Beijing was dominated by a large-scale warm and humid south airflow. The warmest center was located within the built-up area, exhibiting a UHI intensity of approximately 1.2ºC. At 20:00 BJT
230 (Figure 8c), the squall line system that had originated from Taihang Mountain began to enter the northwest edge of the built-up area, creating a cold pool on the ground. The maximum wind speed at the front of this cold pool reached 7.1 m/s. A distinct convergence line was observed between the outflow boundary of the cold pool and the southerly winds of the environmental field in the west of the built-up area. This convergence line followed a northeast-southwest trajectory overall. The convergence zones triggered strong vertical upward movement of airflow in the lower layer, leading to 337 CG
235 lightning events in areas where the temperature gradient zones were most pronounced.

At 21:00 BJT (Figure 8d), as the thunderstorm system developed eastward, the cold pool area expanded further. The maximum wind speed at the front of the cold pool reached 10.4 m/s, and 417 flashes occurred around temperature gradient zones. It was worth noting that at this time the outflow boundary became bifurcated at the edge of the built-up area, and the convergence line began to fragment. At 22:00 BJT (Figure 8e), the outflow angle of the cold pool expanded further. Under
240 the influence of the bifurcated airflow, two cold tongues emerged on the west side of the built-up area. The convergence line broke completely, leading to a significant barrier effect. At this time, SGLNET only recorded 54 lightning flashes near the split convergence line. At 23:00 BJT (Figure 8f), the thunderstorm cell continued to propagate in the built-up area, and SGLNET registered 181 CG lightning events within the built-up area. These findings indicated that when a thunderstorm system passes over a built-up area, the barrier effect caused the cold pool to separate and the convergence line to break.
245 Therefore, the evolution of near-surface cold pools and convergence lines could serve as diagnostic indicators to understand how urban morphologies affected CG lightning activity and the thunderstorm process.

3.3 Numerical simulation of the influence of urban morphologies on the thermal-dynamic structure of thunderstorms

This section made a comparison between the actual observed values of AWS in the vicinity of the built-up area and the simulated values derived from the control experiments during the simulation period.
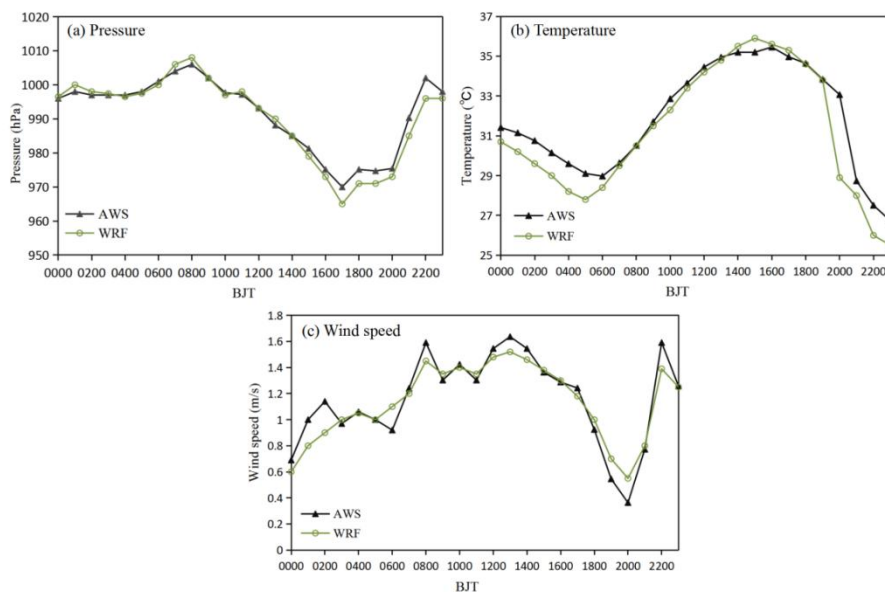
250

Figure 9: Comparison of actual observation and simulation results of the near surface element field for the case "0713", (a) pressure, (b) temperature, and (c) wind speed.

Figure 9 illustrates the simulation error of hourly meteorological elements. As the thunderstorm system progressed towards urban areas (specifically at 20:00), AWS documented a temperature decrease accompanied by an increase in air pressure. At

255 22:00, there was a notable increase in air pressure, a sharp drop in temperature, and a concurrent rapid increase in wind speed. The simulated pressure exhibited a trend similar to that of the observed pressure, with the simulated pressure being 2.1 hPa lower than the observed pressure at 17:00. The curve of the simulated temperature showed a slight lag compared to that of the observed temperature. The variation in simulated wind speed closely mirrored that of the observed temperature, with both showing a rapid increase after 20:00. The emergence of these simulation errors could potentially be attributed to

260 the chosen physical scheme, along with the initial and boundary conditions that were imported. On an overall basis, the simulated ground meteorological field was able to adequately capture the near-surface thermodynamic characteristics associated with the "0713" case.
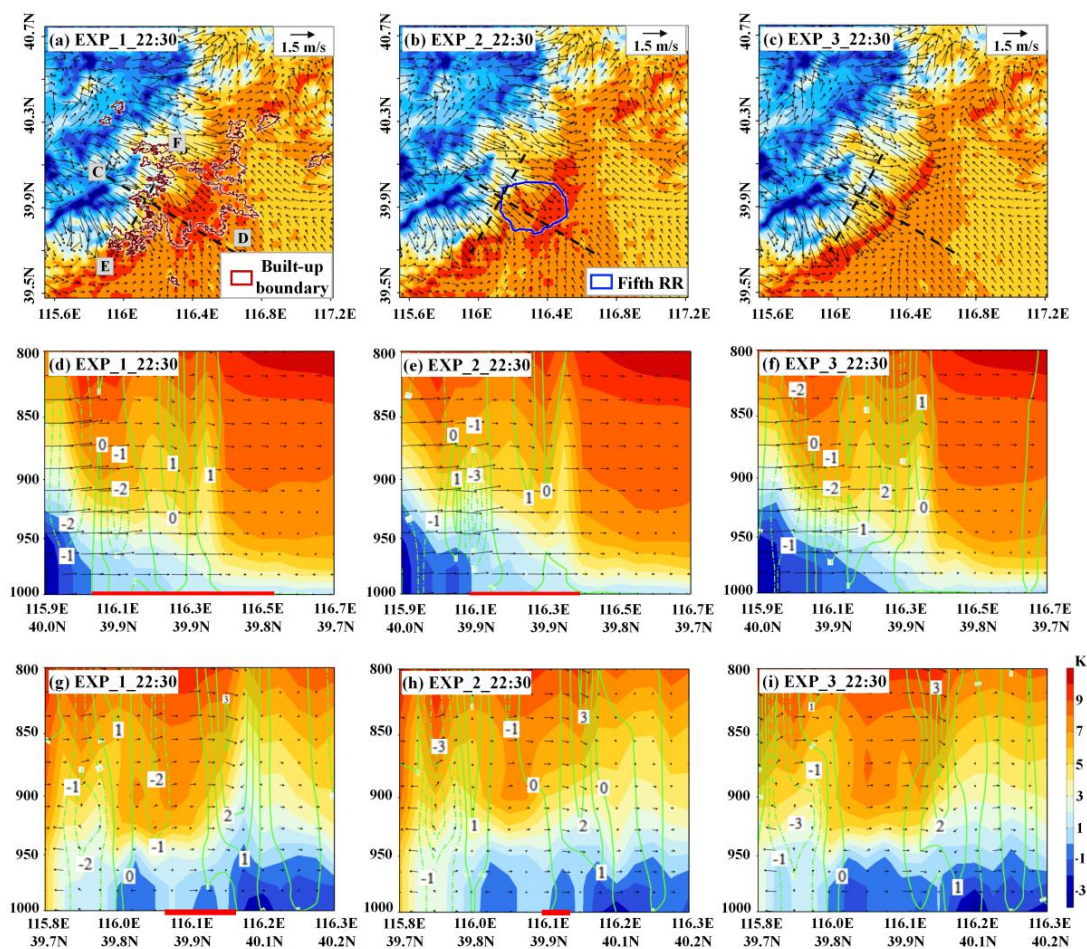
Figure 10: Influence of the scale of the built-up area on near-surface cold pool outflow simulated by WRF. Horizontal thermal-dynamical field (a-c). The cross-sections of perturbation potential temperature (shadow), east-west circulation (vector), and vertical velocity (isoline) along line CD (d-f) and line EF (g-i).

Referring to previous research (Takemi, 2006; Yuan, 2015), this article used a criterion of a perturbation potential temperature lower than -1 K to define the core of the cold pool. The density flow outside this core, which spans a range of -1 K to 1 K, was also defined. The simulation results showed that at 22:30 BJT, as the dry cold air sank and spread, the intensity of the near-surface cold pool increased. The minimum perturbation potential temperature of the cold pool core reached -3 K (Figure 10a). It became evident that as the cold pool approached the edge of the built-up area, the outflow on both sides of the city moved faster, representing that the urban underlying surface dragged the cold pool. A cross section along the line CD (Figure 10d) revealed that due to the barrier effect of the underlying surface, the cold pool accumulated at the edge of the city, with a core thickness of approximately 0.5 km. The urban surface altered the motion of the cold pool, making the cold pool unable to maintain a smooth and continuous shape, and then it bifurcated. A cross-section along line

EF (Figure 10g) revealed that the cold pool was divided into three relatively independent cores, with a more significant thickness at the edge of the city compared to its inner regions. At this time, the influence of the urban underlying surface on the thunderstorm process was dominated by the barrier effect.

280 The length and area of the built-up area in Beijing are approximately 98.6 km and 600 km^2, respectively. In the experimental simulation EXP2, buildings outside the 5th Ring Road were replaced with bare land (Figure 10e), which weakened the accumulation of the cold pool, resulting in a thickness of less than 0.4 km. This led to an increase in vertical speed over the city center and a mitigation of the separation of the cold pool (Figure 10h). When all built-up areas were replaced with bare land in EXP3 (Figure 10c), the accumulation of cold pool cores disappeared (Figure 10f). The cold pool cores exhibited a

285 complete and continuous shape, with vertical upward movement continuing to increase, and the barrier effect almost disappeared.
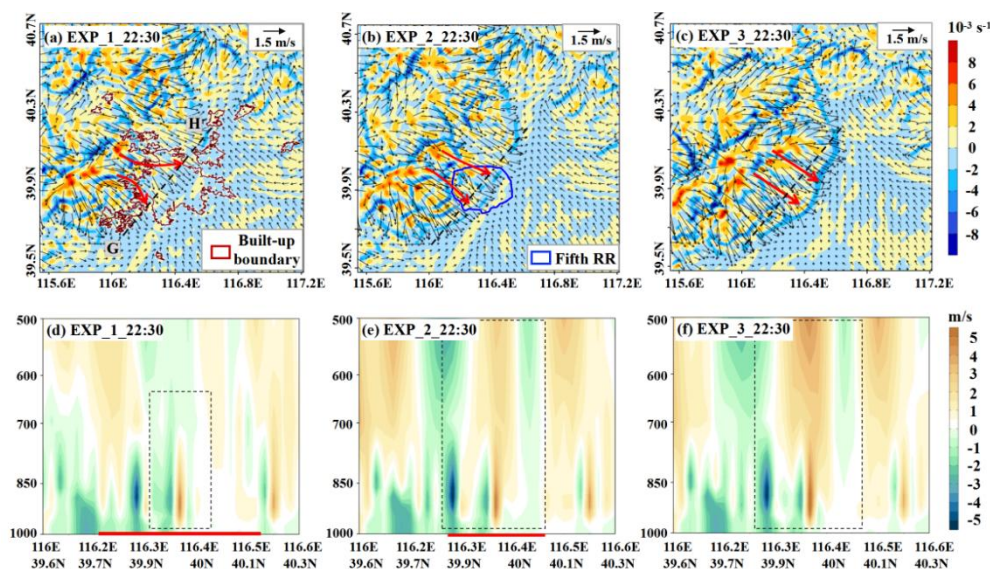
Figure 11: Influence of scale of the built-up area on near-surface convergence zones simulated by WRF. Horizontal wind field and divergence field (a-c). The cross-sections of vertical velocity along line GH (d-e).

290

In EXP1 (Figure 11a), the maximum wind speed at the front of the cold pool outflow reached approximately 5 m/s. Here, the outflow boundary of the cold pool converged with the southerly winds of the environmental field, while divergence zones formed at the center of the built-up area. The gust front at the exit of the cold pool exhibited bifurcation, with one segment southward and the other northward, leaving a sparse outflow in the middle. Figure 11d illustrated that the vertical ascending

295 zone above the city center (denoted by the black dotted rectangle) aligned with the middle segment of the cold pool outflow, though its range and intensity were smaller compared to those at the edge of the city. In contrast, under the conditions of EXP2 (Figure 11b), where the roughness of the urban underlying surface was diminished, the cold pool outflow exhibited a slight bifurcation. This resulted in relatively intact convergence zones within the built-up area. The vertical ascending zone over the city center expanded in range, with a maximum vertical velocity reaching about 4 m/s. In EXP3 (Figure 11c), the

300   maximum wind speed at the front of the cold pool outflow surpassed 8 m/s. The cold pool outflow completely traversed the

built-up area, leading to a further enhancement of the range and intensity of the convergence zones, with a vertical velocity

of 5 m/s. The above results showed that the scale of the built-up area could directly alter the strength of the barrier effect.

This section then further investigated the impact of building density on the barrier effect. In EXP4 (Figure 12a), all types of

building were designated as open-rise. Examination of the simulated dynamic field revealed that the bifurcation angle, the

305   structure of the convergence zone, and the vertical velocity of the cold pool outflow were largely consistent with those

observed in EXP1. In EXP5 (Figure 12c), all types of buildings were set as compact-rise. In particular, the separation angle

of the cold pool outflow was larger than in EXP1, and the vertical velocity was smaller, indicating a more significant barrier

effect. Therefore, it became evident that during summer thunderstorms, the specific morphological characteristics of the

built-up area could significantly modulate the thunderstorm process.
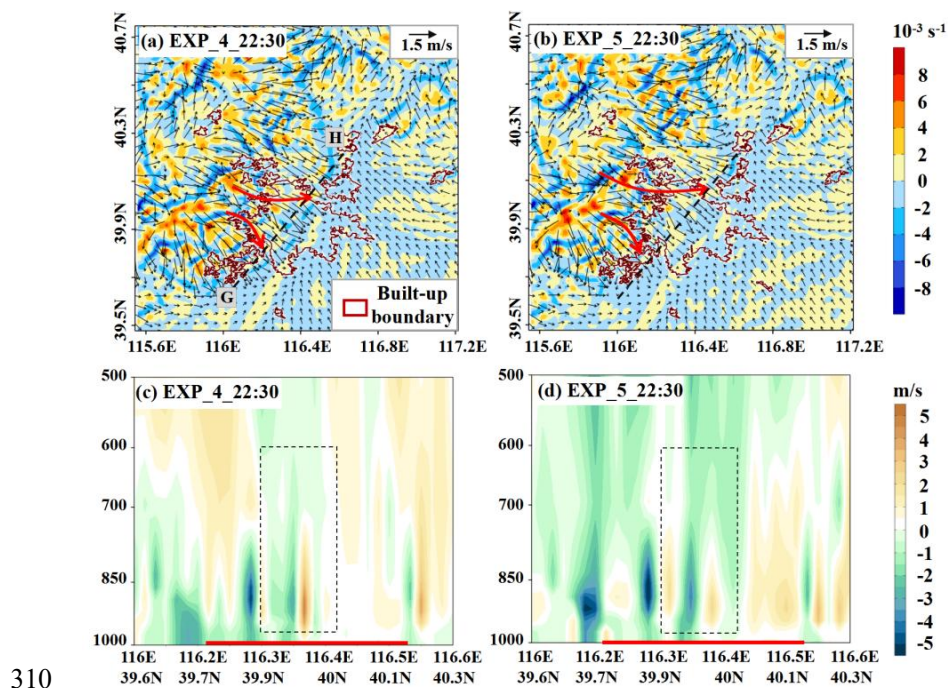
310

Figure 12: Influence of the density of the built-up area on near-surface convergence zones simulated by WRF. Horizontal wind field and divergence field (a-b). The cross-sections of vertical velocity along line GH (c-d).

4 Discussion

This section discussed the mechanism of urban morphology modulation of the CG lightning activity and thunderstorm

315   process, focusing on the thermal-dynamic fields in the middle and lower layers.

As Figure 13a revealed, when thunderstorms passed through the small-scale built-up area, the urban barrier effect on the

flow field was constrained. The horizontal temperature gradient between the cold pool outflow and the urban underlying

surface generated vertical shear of wind speed (Weisman et al., 1984; Chen et al., 2012). This resulted in an increase in

vertical airflow velocity, leading to a forward tilt of the main body of the thunderstorm, thereby ensuring the continuation of

320   ascending airflow (Knaff et al., 2004). Furthermore, the thermal circulation activated by the urban heat island (UHI) contributed to the sustained development and organization of the thunderstorm system. Consequently, when the thunderstorm system encountered the small-scale built-up area, the urban underlying surface enhanced the thunderstorm process primarily through its thermal influence. As a result, CG lightning activity was predominantly concentrated within the built-up area.
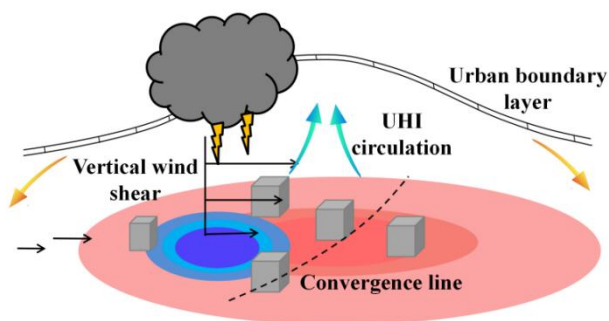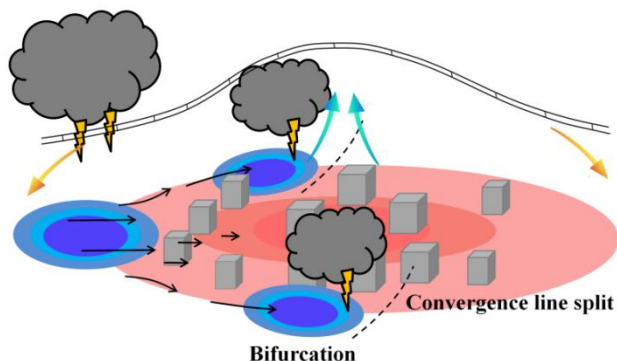
325

Figure 13: The influence mechanism of the barrier effect to alter CG lightning activity and thunderstorm process.

As illustrated in Figure 13b, the rough underlying surface in a large-scale built-up area caused significant attenuation of the horizontal dynamic field (Jin and Shepherd, 2005; Hand and Shepherd, 2009). The urban underlying surface altered the

330   motion state of the cold pool, leading to stagnation and accumulation at the edge of the built-up area. Once the built-up area reached a certain scale, the cold pool outflow separated, and the convergence line broke down. Consequently, the vertical airflow velocity above the built-up area was significantly weakened, preventing the formation of new convective cells. The propagation speed of the thunderstorm cells above the built-up area was slower than on both sides of the city, resulting in bifurcation and movement around the thunderstorm system. Furthermore, as the density of the built-up area increased, the

335 barrier effect became more pronounced. Therefore, when the thunderstorm system passed through the large-scale built-up area, urban morphologies dominated the organization of the thunderstorm process, leading to the concentrated activity of CG lightning at the periphery of the city.

5 Conclusion

Using observation data and numerical simulations, this article conducted a detailed investigation of urban morphology
340 modulation of CG lightning activity and thunderstorm processes. To accomplish this, a thunderstorm case that passed over the populated area of Beijing was selected as a representative for analysis.

Under similar climate conditions, the long-term pattern of the CG lightning activity showed that Beijing and Tianjin, with their extensive urban scales, exhibited a notable barrier effect, while Zhangjiakou, with the smallest urban scale, did not exhibit a barrier effect. When the thunderstorm passed over the city, the evolution of the near-surface cold pool and
345 convergence line provided diagnostic indicators of the influence mechanism of urban morphologies on the lightning activity of CG and the thunderstorm process. Our simulation results further indicated that the urban underlying surface altered the motion state of the cold pool and weakened vertical airflow within the built-up area. Notably, the strength of the barrier effect varied with city size and building density. Finally, this paper established a conceptual model that illustrated how specific urban morphologies modulated the pattern of CG lightning activity and the evolution of thunderstorm processes.

350 Under the background of rapid urbanization, exploring the influence mechanism of urban morphologies on the CG lightning activity and thunderstorm process is highly significant and practical. To achieve a more comprehensive understanding of this relationship, we have planned to utilize unconventional data sources such as microwave radiometers and atmospheric electric field instruments, enabling us to analyze the impact of underlying surfaces on CG lightning activity and thunderstorm processes under different levels of urbanization.

355

Author contributions. Tao, S., Yuanjian, Y. and Gaopeng, L. conceptualized the study. Zuofang, Z. performed the model development, conducted the simulations. Tao, S. wrote the original manuscript and plotted all the figures. Yucheng, Z., Ye, T., Lei, L., and Simone, L. assisted in the conceptualization and model development. All the authors contributed to the manuscript preparation, discussion, and writing.

360 **Acknowledgments.** The data that support the findings of this study are available from the Institute of Urban Meteorology, China Meteorological Administration and the State Grid Electric Power Research Institute, upon applying for cooperation.

Financial support. This research was funded by the National Natural Science Foundation of China (42105147, 41875006, U1938115, and 41775078), the National Key Research and Development Program (2017YFC1501501).

365

Competing interests. The contact author has declared that none of the authors has any competing interests.

References

Bornstein, R., and LeRoy M.: Urban barrier effect on convective and frontal thunderstorms. Preprints, Fourth Conf. on Mesoscale Processes, Boulder, CO, American Meteorological Society, 120–121, 1990.

370 Chen, L., Zhang, Y., Lu, W., Zheng, D., Zhang, Y., Chen, S., and Huang, Z.: Performance Evaluation for a Lightning Location System Based on Observations of Artificially Triggered Lightning and Natural Lightning, Journal of Atmospheric and Oceanic Technology, 29, 1835-1844, http://doi.org/10.1175/JTECH-D-12-00028.1, 2012.

Chen, M., and Wang, Y.: Numerical simulation study of interactional effects of the low-level vertical wind shear with the cold pool on a squall line evolution in North China, Acta Meteorologica Sinica, 70, 3, 371–386,
375 https://doi.org/10.11676/qxxb2012.033, 2012.

Dai, J., Qin, H., and Zheng, J.: Analysis of lightning activity over the Yangtze River Delta using TRMM/LIS observations, Journal of Applied Meteorological Science, 16, 6, 728–736, https://doi.org/10.3969/j.issn.1001-7313.2005.06.003, 2005.

Dou J., Wang, Y., Bornstein, R., and Miao, S.: Observed Spatial Characteristics of Beijing Urban Climate Impacts on Summer Thunderstorms, Journal of Applied Meteorological Science, 54, 1, 94–105, https://doi.org/10.1175/JAMC-D-13-
380 0355.1, 2015.

Farias, W., Pinto, O., Pinto, I., and Naccarato, K.: The influence of urban effect on lightning activity: Evidence of weekly cycle, Atmospheric Research, 135-136(jan.), 370–373, https://doi.org/10.1016/j.atmosres.2012.09.007, 2014.

Hand, L. M., Shepherd, J. M.: An investigation of warm-season spatial rainfall variability in Oklahoma city: possible linkages to urbanization and prevailing wind, Journal of Applied Meteorology And Climatology, 48, 2, 251–269,

385   https://doi.org/10.1175/2008JAMC2036.1, 2009.

Janjic, Z.: The step-mountain eta coordinate model: further developments of the convection, viscous sublayer, and turbulence closure schemes, Monthly Weather Review, 122, 927–945, https://doi.org/10.1175/1520-0493(1994)1222.0.CO;2, 1994.

Jin, M. L., Shepherd, J. M.: Inclusion of urban lands CAPE in a climate model: how can satellite data help?, Bulletin of the

390   American Meteorological Society, 86, 681–689, https://doi.org/10.1175/BAMS-86-5-681, 2005.

Knaff, J. A., Seseske, S. A., Demaria, J. L., and Demuth, J. L.: On the influences of vertical wind shear on symmetric tropical cyclone structure derived from AMSU, Monthly Weather Review, 132, 10, 2503–2510, https://doi.org/10.1175/1520-0493(2004)1322.0.CO;2, 2004.

Lacono, M., Delamere, J., Mlawer, E., Shephard, M. W., And, S. A. C., and Collinset, W. D.: Radiative forcing by long-

395   lived greenhouse gases: calculations with the AER radiative transfer models, Journal of Geophysical Research-Atmospheres, 113, D13103, https://doi.org/10.1029/2008JD009944, 2008.

Lim, K., and Hong, S.: Development of an effective double-moment cloud microphysics scheme with prognostic cloud condensation nuclei (CCN) for weather and climate models, Monthly Weather Review, 138, 1587–1612, https://doi.org/10.1175/2009MWR2968.1, 2010.

400   Lorenz, J. M., Kronenberg, R., Bernhofer, C., and Niyogi, D.: Urban rainfall modification: observational climatology over Berlin, Germany, Journal of Geophysical Research: Atmospheres, 124, 2, 731–746, https://doi.org/10.1029/2018JD028858, 2019.

Markowski, P. M., Straka, J. M., and Rasmussen, E. N.: Direct surface thermal-dynamic observations within the rear-flank downdrafts of nontornadic and tornadic supercells, Monthly Weather Review, 130, 1692–1721,

405   https://doi.org/10.1175/1520-0493(2002)1302.0.CO;2, 2002.

Melin, H., Bormin, H., and Hung-Lung, A. H.: Acceleration of the WRF Monin-Obukhov-Janjic surface layer parameterization scheme on an MIC-based platform for weather forecast, IEEE Journal of Selected Topics in Applied Earth Observations and Remote Sensing, 10, 4399–4408, https://doi.org/10.1109/JSTARS.2017.2725743, 2017.

Miao, S., Chen, F., Li, Q., and Fan, S.: Impacts of urban processes and urbanization on summer precipitation: a case study of

410   heavy rainfall in Beijing on August 1st 2006, Journal of Applied Meteorology and Climatology, 50, 4, 806–825, https://doi.org/10.1175/2010JAMC2513.1, 2011.

National Bureau of Statistics of the People's Republic of China: China statistical yearbook 2021, Beijing, China Statistics Press, 2021.

Orville, R. E., Huffines, G. R., Burrows, W. R., Holle, R. L., and Cummins, K. L.: The north American lightning detection

415   network (NALDN)-first results: 1998-2002, Monthly Weather Review, 130, 2098–2109, https://doi.org/10.1175/1520-0493(2002)130<2098:TNALDN>2.0.CO;2, 2002.

Pinto, I.R.C.A., Pinto, O., Rocha, R.M.L., Diniz, J.H., Carvalho, A.M., and Filho, A.C.: Cloud-to-ground lightning in southeastern Brazil in 1993: Time variations and flash characteristics, Journal of Geophysical Research: Space Physics, 104, 31381–31387, https://doi.org/10.1029/1999JD900799, 1999.

420 Qie, X., Yuan, S., Chen, Z., Wang, D., Liu, D., Sun, M., Sun, Z., Srivastava, A., Zhang, H., Lu, J., Xiao, H., Bi, Y., Feng, L., Tian, Y., Xu, Y., Jiang, R., Liu, M., Xiao, X., Duan, S., Su, D., Sun, C., Xu, W., Zhang, Y., Lu, G., Zhang, D., Yin, Y., and Yu, Y.: Understanding the dynamical-microphysical-electrical processes associated with severe thunderstorms over the Beijing metropolitan region, Science China Earth Sciences, 64, 1, 1–17, http://doi.org/10.1007/s11430-020-9656-8, 2021.

425 Schulz, W., Cummins, K., Diendorfer, G., Dorninger, M.: Cloud-to-ground lightning in Austria: A 10-year study using data from a lightning location system, Journal of Geophysical Research: Space Physics, 110, D9, D09101, https://doi.org/10.1029/2004JD005332, 2005.

Shepherd, J M, and Burian S J.: Detection of urban-induced rainfall anomalies in a major coastal city, Earth Interact, 7, 4, 1–17, https://doi.org/10.1175/1087-3562(2003)007<0001:douira>2.0.co;2, 2003.

430 Shi, T., Yang, Y., Zheng, Z., Tian, Y., Huang, Y., Lu, Y., Shi, C., Liu, L., Zi, Y., Wang, Y., Wang, Y., Lu, G., and Wang, G.: Potential urban barrier effect to alter patterns of cloud-to-ground lightning in Beijing metropolis, Geophysical Research Letters, 49, e2022GL100081, https://doi.org/10.1029/2022GL100081, 2022.

Stallins, J. A., and Bentley, M. L.: Urban lightning climatology and GIS: An analytical framework from the case study of Atlanta, Georgia, Applied Geography, 26, 3–4, 242–259, https://doi.org/10.1016/j.apgeog.2006.09.008, 2006.

435 Stewart, I. D., and Oke, T. R.: Local Climate Zones for Urban Temperature Studies, Bulletin of the American Meteorological Society, 93, 12, 1879–1897, http://doi.org/10.1175/BAMS-D-11-00019.1, 2012.

Sun, J., He, N., Guo, R., and Chen, M.: The Configuration Change and Train Effect Mechanism of Multi-Cell Storms, Chinese Journal of Atmospheric Sciences, 37, 1, 137–148, https://doi.org/CNKI:SUN:DQXK.0.2013-01-014, 2013.

Sun, J., and Yang, B.: Meso-β Scale Torrential Rain Affected by Topography and the Urban Circulation, Chinese Journal of
440 Atmospheric Sciences, 32, 6, 1352–1364, https://doi.org/10.3878/j.issn.1006-9895.2008.06.10, 2008.

Sun, X., Luo, Y., Gao X., Wu, X., and Xu, H.: On the Localized Extreme Rainfall over the Great Bay Area in South China with Complex Topography and Strong UHI Effects, Monthly Weather Review, 149, 8, 2777–2801, https://doi.org/10.1175/MWR-D-21-0004.1, 2021.

Takemi, T.: Impacts of moisture profile on the evolution and organization of mid-latitude squall lines under various shear
445 conditions, Atmospheric Research, 82, 1-2, 37–54, https://doi.org/10.1016/j.atmosres.2005.01.007, 2006.

Tewari, M., Chen, F., Wang, W., Dudhia, J., and Cuenca, H.: Implementation and verification of the unified NOAH land surface model in the WRF model, 20th conference on weather analysis and forecasting/16th conference on numerical weather prediction, pp.11–15, 2004.

Wang, Q., Li, Zb., Guo, J., Zhao, C., and Cribb, M.: The climate impact of aerosols on the lightning flash rate: Is it
450   detectable from long-term measurements?, Atmospheric Chemistry Physics, 18, 17, 12797–12816,
https://doi.org/10.5194/acp-18-12797-2018, 2018.

Wang, Y., Lu, G., Shi, T., Ma, M., and Wang, Y.: Enhancement of Cloud-to-Ground Lightning Activity Caused by the
Urban Effect: A Case Study in the Beijing Metropolitan Area, Remote Sensing, 13, 7, 1228, https://doi.org/doi:
10.3390/rs13071228, 2021.

455   Weisman, M. L., and Klemp, J. B.: The structure and classification of numerically simulated convective storms in
directionally varying wind shears, Monthly Weather Review, 112, 12, 2479–2498, https://doi.org/ 10.1175/1520-
0493(1984)112<2479:TSACON>2.0.CO;2, 1984.

Westcott, N. E.: Summertime Cloud-to-Ground Lightning Activity around Major Midwestern Urban Areas, Journal of
Applied Meteorology, 34, 7, 1633–1642, https://doi.org/10.1175/1520-0450-34.7.1633, 1995.

460   Xiao, X., Sun, J., Chen, M., Qie, X., and Ying, Z.: The characteristics of weakly forced mountain-to-plain precipitation
systems based on radar observations and high-resolution reanalysis, Journal of Geophysical Research-Atmospheres, 122, 6,
3193–3213, https://doi.org/10.1002/2016JD025914, 2017.

Xu, R., Miao, J., and Tan, Z.: Numerical Simulation of the Impact of Urban Underlying Surface Characteristics on
Thunderstorm in Nanjing, Chinese Journal of Atmospheric Sciences, 37, 6, 1235–1246,
465   https://doi.org/10.3878/j.issn.1006-9895.2012.12128, 2013.

Xu, W. H., Li, Q., Wang, X., S Yang, Cao, L., and Feng, Y.: Homogenization of Chinese daily surface air temperatures and
analysis of trends in the extreme temperature indices, Journal of Geophysical Research: Atmospheres, 118, 17, 9708–9720,
https://doi.org/10.1002/jgrd.50791, 2013.

Yang, L., Li, Q., Yuan, H., Niu, Z., and Wang, L.: Impacts of urban canopy on two convective storms with contrasting
470   synoptic conditions over Nanjing, China, Journal of Geophysical Research: Atmospheres, 126, 9, e2020JD034509,
https://doi.org/10.1029/2020JD034509, 2021.

Yin, J., Zhang, D., Luo, Y., and Ma, R.: On the Extreme Rainfall Event of May 7th 2017 Over the Coastal City of
Guangzhou. Part I: Impacts of Urbanization and Orography, Monthly Weather Review, 148, 3, 955–979,
https://doi.org/10.1175/MWR-D-19-0212.1, 2020.

475   Yuan, Z.: Study of the influence of the different horizontal resolutions and microphysical setups on the idealized simulation
of a squall line, Acta Meteorologica Sinica, 73, 4, 648–666, https://doi.org/10.11676/qxxb2015.049, 2015.

Yue, C., Tang, Y., Gu, W., Han, Z., and Wang, X.: Study of Urban barrier effect on Local Typhoon Precipitation,
Meteorological Monthly, 45, 11, 1611–1620, https://doi.org/CNKI:SUN:QXXX.0.2019-11-011, 2019.

Zhu, Y., Liu, H., and Shen, J.: Influence of Urban Heat Island on Pollution Diffusion in Suzhou, Plateau Meteorology, 35, 6,
480   1584–1594, https://doi.org/10.7522/j.issn.1000-0534.2016.00084, 2016.